Scaling of small-scale motions in wallbounded turbulent flows

Wei, L; Elsinga, Gerrit; Brethouwer, G; Schlatter, P; Johansson, AV

Important note
To cite this publication, please use the final published version (if applicable).
Please check the document version above.

SCALING OF SMALL-SCALE MOTIONS IN WALL-BOUNDED TURBULENT FLOWS

Liang Wei
Linné FLOW Centre, KTH Mechanics
Royal Institute of Technology
100 44 Stockholm, Sweden
wei@mech.kth.se

Gerrit E. Elsinga
Laboratory for Aero and Hydrodynamics
Delft University of Technology
2628CA Delft, The Netherlands
G.E.Elsinga@tudelft.nl

Geert Brethouwer
Linné FLOW Centre, KTH Mechanics
Royal Institute of Technology
100 44 Stockholm, Sweden
geert@mech.kth.se

Philipp Schlatter
Linné FLOW Centre, KTH Mechanics
Royal Institute of Technology
100 44 Stockholm, Sweden
pschlatt@mech.kth.se

Arne V. Johansson
Linné FLOW Centre, KTH Mechanics
Royal Institute of Technology
100 44 Stockholm, Sweden
johansson@mech.kth.se

ABSTRACT

The objective is to investigate flow topology and related Reynolds-number scaling in the eigenframe of the strain-rate tensor for wall-bounded turbulent flows. The databases used in the current study are from direct numerical simulations (DNS) of fully developed channel flow up to friction Reynolds number $Re_\tau \approx 1500$, and a spatially developing, zero-pressure-gradient turbulent boundary layer up to $Re_\theta \approx 4300$ ($Re_\tau \approx 1400$). It is found that for all cases considered, the averaged flow patterns in the local strain-rate eigenframe appear universal: large scale motions are separated by a shear layer with a pair of vortices. Based on Kolmogorov (η, u_η), Taylor (l_t) and integral length scales, Reynolds-number scalings of the averaged flow patterns, including the thickness and strength of the shear layer, the distance between the two vortical regions, and the velocity distribution along the most compressing and stretching directions are considered. It is found that the Taylor scaling of the profiles for the thickness of the shear layer seems more suitable than the Kolmogorov scaling, and the integral scaling collapses well away from the shear layer, which confirms that those patterns represent large scales. Generally speaking, the scaling profiles based on the Kolmogorov length and velocity collapse well near the origin, but the Taylor scaling seems best suited in a broader region.

1 Introduction

Turbulent flows are usually characterized by a broad range of scales (the higher the Reynolds number, the broader the range of scales), where large scales are flow dependent, but small scales show some universal character-istics. This universality has led to the development of turbulence modeling like large-eddy simulation (LES). The aim of the present work is to investigate the universality and its related Reynolds-number scaling for different types of wall-bounded turbulent flows.

Many studies have been done to discover and understand the universal features of small-scale turbulent motions. Ashurst *et al.* (1987) simulated isotropic turbulence and homogeneous shear flow with Reynolds numbers of around 83 based on the Taylor microscale. It was found that there was a preferential alignment of the vorticity vector with the intermediate strain direction. They argued that the alignment was a consequence of angular momentum conservation. Jiménez (1992) offered another explanation for the alignment using a kinematic model and attributed it to purely kinematic effects. Chong *et al.* (1990) proposed a topology classification for three dimensional flow fields using tensor invariants P, Q, R, in which four different regions were categorized in the *Q-R* space. Blackburn *et al.* (1996) studied fine-scale motions in turbulent channel flow and confirmed the teardrop shape of joint probability-density function (p.d.f.) of *Q-R* and the alignment of the vorticity vector and the intermediate eigenvector of the strain-rate tensor. More recently, Elsinga & Marusic (2010) proposed a method to extract average flow patterns in a local frame of reference defined by the eigenvectors of the strain rate tensor and applied the method to three turbulent flow cases: a turbulent boundary layer, a turbulent channel flow, and homogeneous isotropic turbulence. It was found that for all three cases the average pattern showed a shear layer structure separating two larger-scale, relatively uniform regions.

The Reynolds number has a great effect on turbulence

motions, especially the size of the smallest scales. Turbulent flows with a broad range of Reynolds numbers are needed for a further study of the universality of small-scale turbulence motions. The current work uses the averaging scheme proposed by Elsinga & Marusic (2010) (with slightly different local coordinate systems) in the strain-rate eigenframe to investigate the universality of turbulent boundary layer and channel flows with different Reynolds numbers and the related Reynolds-number scalings. One big difference between turbulent boundary layer and channel flows is that the former exhibit a large degree of intermittency in the outer region (Corrsin & Kistler, 1955). This study will be focused on the turbulence-dominated region.

2 Methodology

The strain-rate eigenframe of reference is chosen to evaluate the flow field statistically, mainly because this frame of reference is associated with some universal features of small-scale turbulence like the preferential alignment between the vorticity vector $\boldsymbol{\omega}$ and the intermediate principal straining direction, and in addition, the invariants of the velocity gradient tensor (Q, R) are also linked, in part, to principal straining. The strain-rate tensor, $S_{ij} = 0.5 * (\partial u_i / \partial x_j + \partial u_j / \partial x_i)$, has three eigenvalues ($\lambda_1 > \lambda_2 > \lambda_3$) and respective three eigenvectors ($\boldsymbol{\lambda}_1$, $\boldsymbol{\lambda}_2$, and $\boldsymbol{\lambda}_3$), which are orthogonal due to the symmetry of S_{ij}. For incompressible flows $\lambda_1 > 0$ and $\lambda_3 < 0$. $\boldsymbol{\lambda}_1$ and $\boldsymbol{\lambda}_3$ represent the most stretching and compressing directions, respectively. The direction of $\boldsymbol{\omega}$ at different points in a flow field is different, however, it is often aligned with $\boldsymbol{\lambda}_2$, as shown by many studies (e.g. Ashurst *et al.*, 1987; Jiménez, 1992; Blackburn *et al.*, 1996; Elsinga & Marusic, 2010). If the flow field around each point is mapped along the local $\boldsymbol{\lambda}_1$, $\boldsymbol{\lambda}_2$, $\boldsymbol{\lambda}_3$ directions, a local flow field is obtained as it is viewed from an observer aligned with the local eigenframe. We may expect to see some common features associated with the local strain field and it is interesting to investigate their statistical structures both qualitatively and quantitatively.

Specifically, the point-wise statistics collecting method in the local strain-rate eigenframe consists of the following steps (see figure 1 for a 2D illustration): 1) Choose a global measurement volume (G) in a turbulent region of a flow field. 2) Compute $\boldsymbol{\lambda}_1$, $\boldsymbol{\lambda}_2$, and $\boldsymbol{\lambda}_3$ of S_{ij} at one point, e.g. A. Typically the $\boldsymbol{\lambda}_3$ direction is adjusted to maintain a right-handed system, after $\boldsymbol{\lambda}_2$ and $\boldsymbol{\lambda}_1$ are fixed (Note that the principal straining axes do not have a positive direction defined. Therefore one may define a positive direction, for instance, based on the vorticity and the $\boldsymbol{x}$-direction). $\boldsymbol{\lambda}_2$ is chosen to point to the positive $\boldsymbol{\omega}$, the same as Elsinga & Marusic (2010). The different part is that $\boldsymbol{\lambda}_1$ is also made aligned with the positive $\boldsymbol{x}$ direction (the dot product of $\boldsymbol{\lambda}_1$ and $\boldsymbol{x}$ is positive). 3) Create a uniform grid in the local coordinate system originated at A with three principal directions along $\boldsymbol{\lambda}_1$, $\boldsymbol{\lambda}_2$, and $\boldsymbol{\lambda}_3$. 4) Map the global fluctuating velocity field around A onto the local uniform grid to get the local velocity field. 5) Apply steps 2–4 to all points in the global volume (G) and average the obtained local velocity fields over the local grid to get the averaged flow patterns.

3 Results and analysis

The databases used in the current study are from direct numerical simulations (DNS) of fully developed channel flow with friction Reynolds numbers up to $Re_\tau \approx$
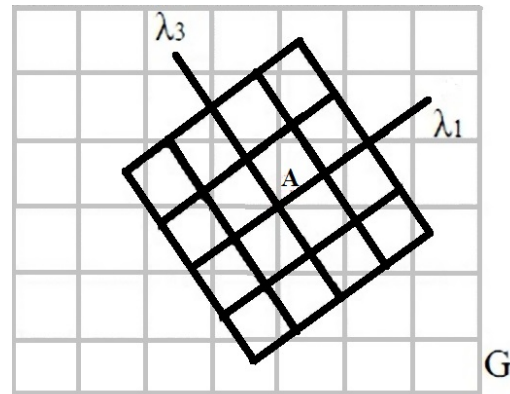

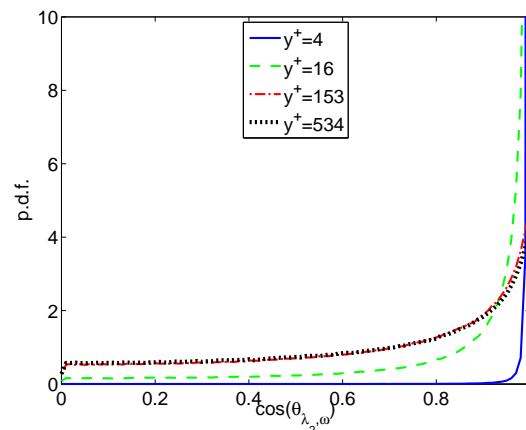Figure 1.   2D illustration of the global and local grids.

Figure 2.   p.d.f. of the angle between λ_2 and ω.

1500, and a spatially developing, zero-pressure-gradient turbulent boundary layer with the Reynolds number up to $Re_\theta \approx 4300$ ($Re_\tau \approx 1400$), based on the momentum thickness θ and free-stream velocity (Schlatter *et al.*, 2009; Schlatter & Örlü, 2010). For comparison/scaling purpose, the Reynolds numbers considered for the current cases are $Re_\tau \approx 550, 1000, 1500/550, 1000, 1350$ for channel and boundary layer flows respectively, and the global measurement volume considered for both type of flows are around $0.3h$ (where h is the half channel width for channel and the boundary layer thickness δ for boundary layer flows), well in the outer region, more specifically, $0.3h$ for channel flow, and 0.22-0.38δ for boundary layer, where turbulence dominates and boundary layer intermittency is negligible.

An essential basis for the current averaging method is the alignment of $\boldsymbol{\lambda}_2$ with $\boldsymbol{\omega}$. It is expected to see the alignment for the current turbulent flow cases. Figure 2 presents the p.d.f. of the cosine of the angle θ between $\boldsymbol{\lambda}_2$ and $\boldsymbol{\omega}$ for channel flow ($Re_\tau \approx 550$) in four different regions: viscous sublayer, buffer layer, log layer, and wake region. It can be seen that the profiles peak at $\theta = 0$ for all regions. The closer to the wall, the higher the peak values, and it gets much higher in the viscous sublayer and buffer layer regions, that is, the regions with high dissipation of turbulent kinetic energy, due to the presence of the wall. Similar results can be found for other Reynolds numbers and boundary layers, and it is in good agreement with the results of Blackburn *et al.* (1996).

Like the alignment, the averaged flow patterns in the

2

local strain-rate eigenframe are similar for all cases. For simplicity, only the results from channel flow at $Re_\tau \approx 550$ are shown here. Figure 3 presents the averaged fluctuating velocity vector field in three different cross planes. Coordinates are normalized using Kolmogorov scale. Two vortical regions inside the shear layer can be seen in the vector field plot on the plane $\lambda_2 = 0$ (λ_1-λ_3 plane), as shown in figure (a). The scaling of this structure will be discussed later in this section. Figures (b) and (c) present the vector plots at $\lambda_3 = 0$ and $\lambda_1 = 0$ planes, respectively. It is obvious to see the stretching in the $\boldsymbol{\lambda_1}$ direction and compression in the $\boldsymbol{\lambda_3}$ direction. The vectors also indicate a weak stretching in the $\boldsymbol{\lambda_2}$ direction, which can also be seen in figure 3(d).

The flow topology can be classified into four different quadrants in the Q-R plane (Chong *et al.*, 1990; Blackburn *et al.*, 1996). The flow patterns in figure 3 mainly fall into two categories: stable focus/stretching, and unstable node/saddle/saddle. It is confirmed by the 2nd and 3rd invariants of the fluctuating velocity gradient tensor Q-R scatter plots shown in figure 4. The green line is the zero-discriminant line $D = 27/4R^2 + Q^3 = 0$, which separates the four quadrants together with the $R = 0$ line. The plot reveals a preference for the 2nd and 4th quadrants, similar for all the current cases, which corresponds to stable focus/stretching and unstable node/saddle/saddle structure (Chong *et al.*, 1990; Blackburn *et al.*, 1996). The averaged flow pattern in the local strain-rate eigenframe directly explains the preference of flow topologies.

The above discussions about the universality of the averaged flow patterns are mainly conducted in a qualitative way. A quantitative study is needed for further evaluating the universality. The averaged flow field has patterns related to flow topology and turbulence scales on which Reynolds number has a significant effect. It will be interesting to investigate this effect which may shed some light on sub-grid scale turbulence modeling LES.

Reynolds-number scalings of the universal flow patterns for all cases are computed using the Kolmogorov (length η and velocity u_η) and Taylor scales ($l_t = \sqrt{\overline{u^2}/\overline{u_x^2}}$, where u is the streamwise fluctuating velocity and $u_x = \partial u/\partial x$), and the integral scale (h). Since the local flow pattern indicates a shear layer with two vortical regions, as indicated in figure 3(a), the scalings will be focused on their parameters, such as the thickness and strength of the shear layer, the distance between the two vortical regions, velocity distributions in the most compressing and stretching directions, which will be discussed below.

The thickness and strength of the shear layer are determined from the profiles of tangential velocities in the vector field at the $\lambda_2 = 0$ plane, that is, along line II in figure 3(a) with its origin located at $\lambda_3 = 0$. The related Reynolds-number scalings using Kolmogorov length/velocity scales, Taylor scale are plotted in figures 5, 6, and 7. It can be seen that the profiles for all the current cases collapse quite well very near the origin for both scalings, but the Taylor scaling seems to perform slightly better away from the origin. They reach their peaks at the same location $\lambda_3 \approx 6\eta$ or $0.28l_t$, which gives the thickness of the shear layer of around 17η or $0.79l_t$ (note that the line is inclined at a 45 degree angle). The Kolmogorov velocity scaling indicates a good collapse of the profiles with a peak velocity around $3.5u_\eta$, shown in figure 7. The shear layers share a universal thickness and strength for both turbulent channel and boundary layer flows. The quantitative universality extends up to about 1 Taylor scales, after which the profiles start to deviate. In
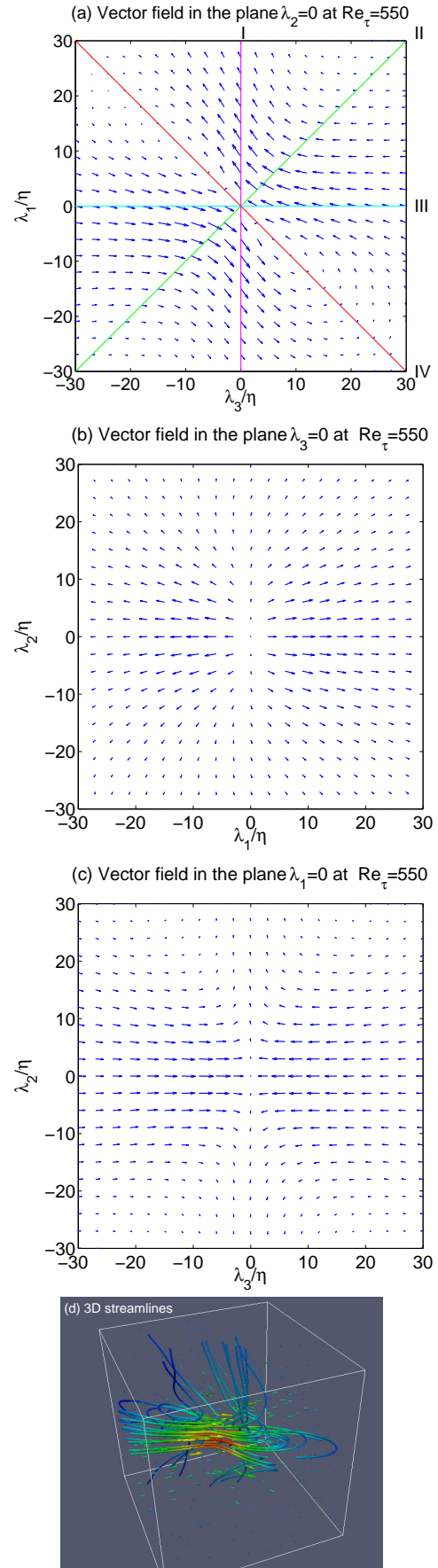
Figure 3. Averaged fluctuating velocity field (a,b,c) and 3D streamlines (d) in the local strain-rate eigenframe for channel flow at $Re_\tau \approx 550$. η is Kolmogorov length scale. Lines I, II, III, and IV in (a) are used for scalings below.
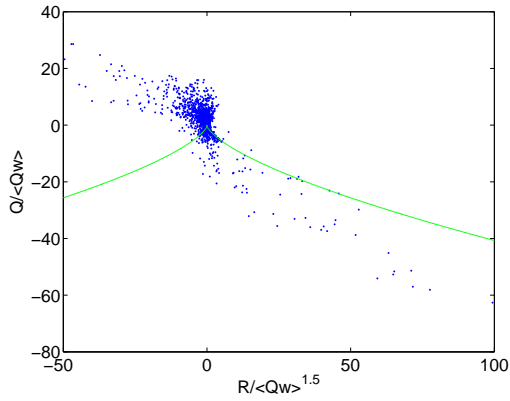
Figure 4. Q-R scatter plots for channel flow at $Re_\tau \approx 550$ in the local strain-rate eigenframe. Q_W is the 2nd invariant of the rotation-rate tensor.
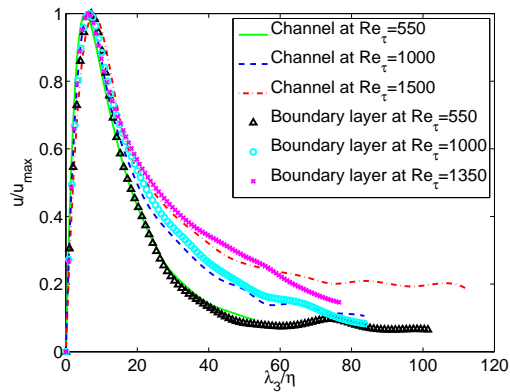

Figure 5. Scaling of the shear layer using Kolmogorov length scale, where u is on the line II in figure 3(a) and tangential to the shear layer, u_{max} is the maximum velocity, the same for figures 6 and 7.
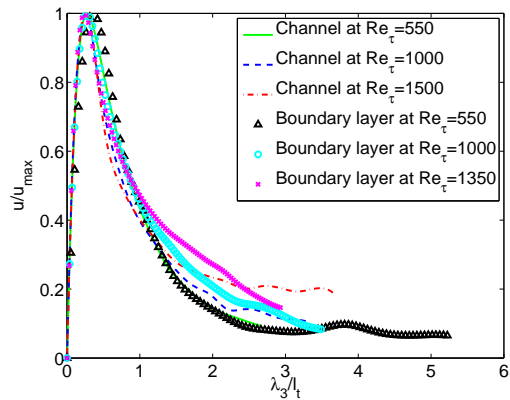

Figure 6. Scaling of shear layer using Taylor scale (l_t).

particular the tail is seen to increase with Reynolds number consistent with the largest scales increasing in size when expressed in Taylor length scales. Moreover, the tail seems flow dependent, as expected for the largest scales. The largest scales are further confirmed by the good collapse of the integral scaling profiles in figure 8.

The distance between the two vortical regions can be obtained through the profiles of perpendicular velocities in
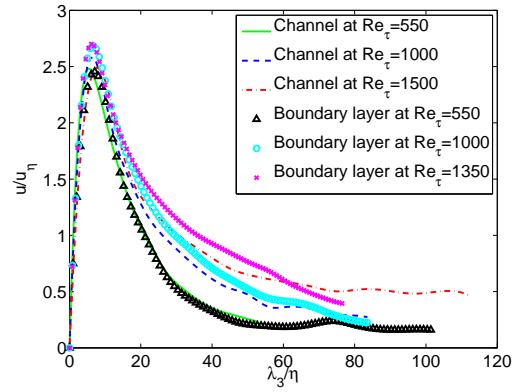

Figure 7. Scaling of shear layer, using Kolmogorov scales. u_η is the Kolmogorov velocity scale.
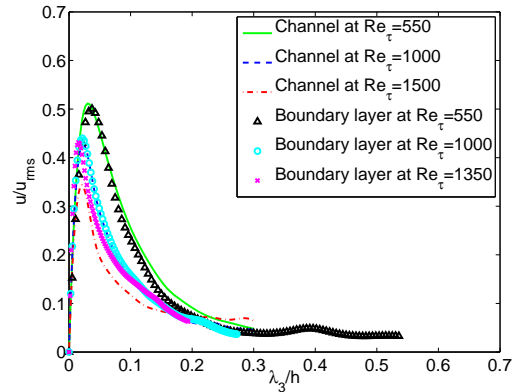

Figure 8. Scaling of shear layer, using integral length scale (h is the half channel width/boundary layer thickness). u_{rms} is root-mean-square of the streamwise velocity.

the vector field at the $\lambda_2 = 0$ plane, i.e., line IV in figure 3(a). The scaling profiles are shown in figures 9, 10, and 11. The peak and zero values of the velocities represent the centre and edge of the vortical regions. It is indicated that the edge location is $\lambda_3 \approx 5\eta$ or $0.21l_t$ with an edge velocity around $0.6u_\eta$, and the centre of the vortical region $\lambda_3 \approx 14\eta$ or $0.58l_t$. This gives a distance of around 39η or $1.64l_t$ between the cores of two vortical regions for all cases, which is similar to the spacing of $1.7l_t$ given by Elsinga & Marusic (2010). The scaling profiles based on the Taylor scale seem to have a slightly better collapse between the cores of two vortices, while both scalings work well between two edges.

The scaling of the velocity distribution in the most compressing (λ_3) and stretching (λ_1) directions (lines III and I in figure 3, respectively) are displayed in figures 12, 13, 14 and 15, 16, 17 respectively. On the one hand, the Kolmogorov scaling gives a nice collapse before reaching the peak location at around 14η, as indicated in figures 12 and 15. On the other hand, the Taylor scaling seems to give a very good collapse in a broader region away from the origin in both λ_3 and λ_1 directions, shown in figures 13 and 16. The Kolmogorov velocity seems to be a suitable scale for stretching and compressing velocities, as indicated in figures 14 and 17 . It is interesting to see that the maximum velocity in the λ_3 direction is slightly higher than the one in the λ_1 direction, which may provide an explanation for the weak stretching in the λ_2 direction.

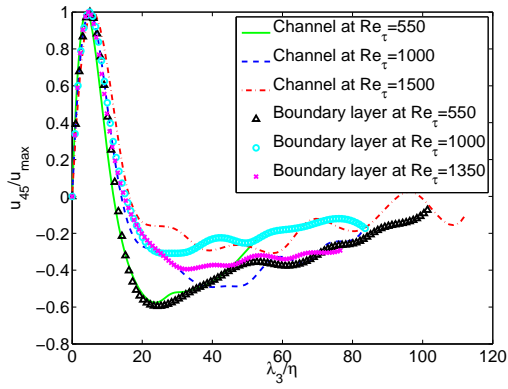It can be seen from the above discussions that the ob-

4

Figure 9. Scaling of the velocity u_{45} on the line IV in figure 3(a) using Kolmogorov length scale, where u_{45} means that the velocity is 45 degree inclined to the λ_3 direction, that is, perpendicular to the shear layer, the same for figures 10 and 11.
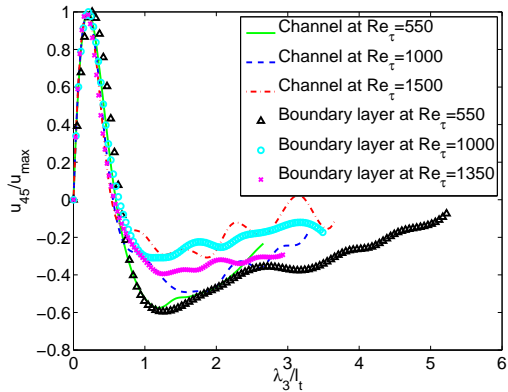

Figure 12. Scaling of the velocity u_3 on the line III in figure 3(a) using Kolmogorov length scale, where, u_3 means the velocity in the λ_3 direction, that is, the most compressing direction, the same for figures 13 and 14.

Figure 10. Scaling of the velocity u_{45} using Taylor scale.

Figure 13. Scaling of the velocity u_3 using Taylor scale.

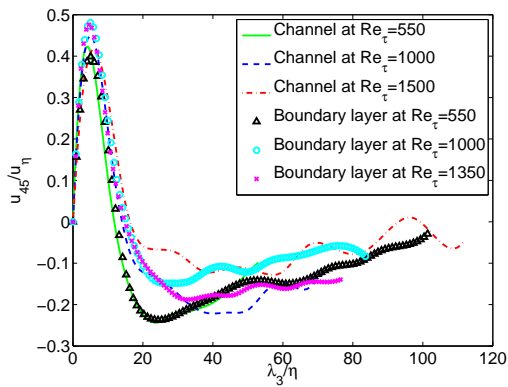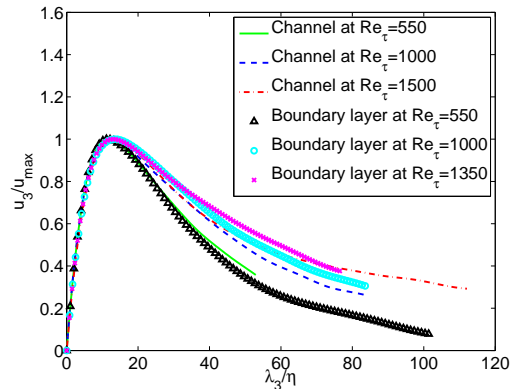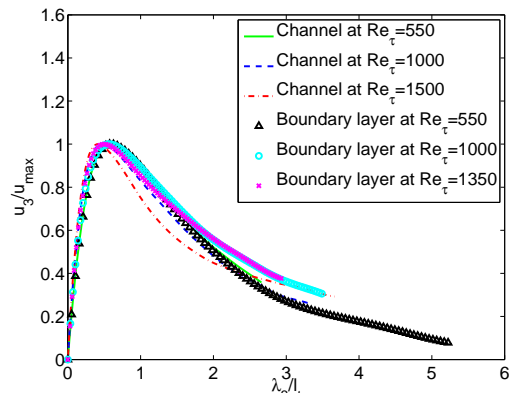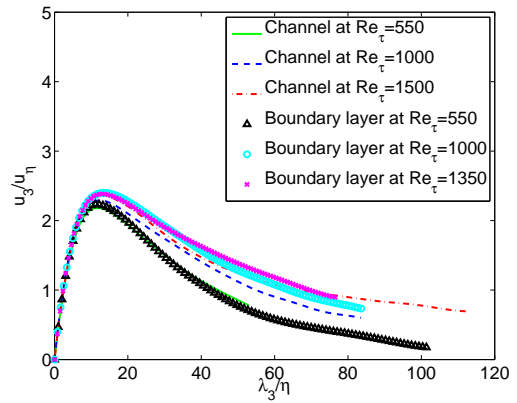Figure 11. Scaling of the velocity u_{45} using Kolmogorov length and velocity scales.

Figure 14. Scaling of the velocity u_3 using Kolmogorov length and velocity scales.

tained shear-layer like structure scales on not only Taylor and Kolmogorov scales, but also the integral length scale, which indicates that the structure represents both small and large scales of turbulence. Kolmogorov scaling performs well near the origin, where viscosity seems important, and Taylor scale appears to have a good collapse in a broader region, while integral length scaling of the shear layer works well further away from the origin, i.e. outside the shear layer. The structure of the shear layer with a thickness of

around 17η or $0.79l_t$ (two aligned vortices with a spacing of $1.64l_t$) separating large scale motions appears universal.

4 Summary

The universality of small-scale turbulence motions in channel and boundary layer flows at different Reynolds numbers and related Reynolds-number scaling has been considered. The friction Reynolds numbers for the
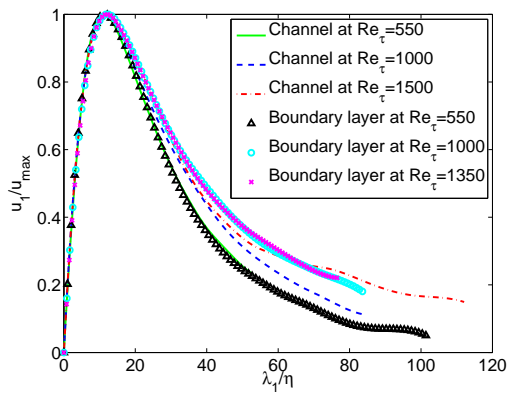
5

Figure 15. Scaling of the velocity u_1 on the line I in figure $3(a)$ using Kolmogorov length scale, where, u_1 means the velocity in the $\boldsymbol{\lambda}_1$ direction, that is, the most stretching direction, the same for figures 16 and 17.
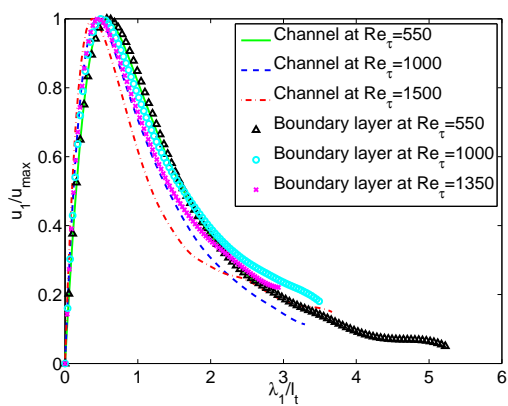

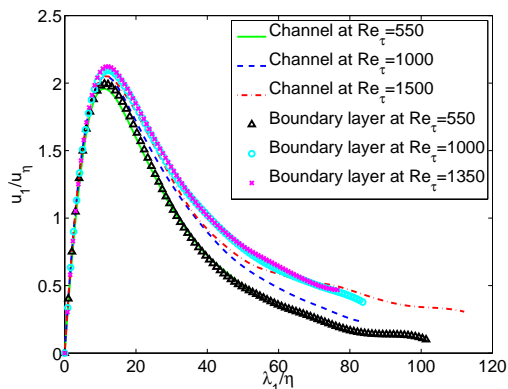Figure 16. Scaling of the velocity u_1 using Taylor scale.

Figure 17. Scaling of the velocity u_1 using Kolmogorov length and velocity scales.

DNS databases are $Re_\tau \approx 550, 1000, 1500$ for channel and $550, 1000, 1350$ for boundary layer. There is a preferential alignment between the vorticity vector and the intermediate straining direction for turbulent flows. The methodology is to map a global flow field around/near a point (in a chosen global measurement volume) onto its local coordinate de-

fined by the eigenvectors of the strain-rate tensor, to obtain a local flow field, and then average the obtained local flow fields for all points in the global volume to get statistically averaged flow patterns around a point.

The alignment between the vorticity vector and the intermediate strain-rate eigenvector was evaluated in the viscous sublayer, buffer layer, log layer, and wake region. It is found from the p.d.f. of the angle between the two vectors that they are well aligned in all regions and the closer to the wall, the closer the alignment, which indicates that the presence of the wall significantly enhances the alignment.

The average flow patterns in the local coordinate appear universal across the wall-bounded flows considered here. It features a shear layer (with two aligned vortices) separating large scale motions which was confirmed by the integral length scaling. It also indicates the preference of 2nd and 4th quadrants for the flow topologies in the Q-R plane, which is also confirmed by the Q-R scatter plots. Since the Reynolds number has a great effect on turbulence scales, a Reynolds-number scaling using Taylor and Kolmogorov length scales, as well as the integral length scale is needed, which can also further quantify its universality. It was found that the Taylor scaling of the profiles for the thickness of the shear layer seems more suitable than the Kolmogorov scaling, while integral length scaling works well away from the shear layer. Generally speaking, for turbulent channel and boundary layer flows at different Reynolds numbers, the features of the local averaged flow field, such as the thickness of the shear layer, the edge/centre location of the vortex, and the velocity distribution along the most compressing and stretching directions scale well with the Kolmogorov length and velocity scales close to the origin while the Taylor scale appears best suited in a broader region.

REFERENCES

Ashurst, W. T., Kerstein, A. R., Kerr, R. M. & Gibson, C. H. 1987 Alignment of vorticity and scalar gradient with strain rate in simulated Navier-Stokes turbulence. *Phys. Fluids* **30**, 2343–2353.

Blackburn, H. M., Mansour, N. N. & Cantwell, B. J. 1996 Topology of fine-scale motions in turbulent channel flow. *J. Fluid Mech* **310**, 269–292.

Chong, M. S., Perry, A. E. & Cantwell, B. J. 1990 A general classification of three-dimensional flow fields. *Phys. Fluids A* **2**, 765–777.

Corrsin, S. & Kistler, A. L. 1955 The free-stream boundaries of turbulent flows. *Tech. Rep.* TR-1244. NACA.

Elsinga, G. E. & Marusic, I. 2010 Universal aspects of small-scale motions in turbulence. *J. Fluid Mech* **662**, 514–539.

Jiménez, J. 1992 Kinematic alignment effects in turbulent flows. *Phys. Fluids A* **4**, 652–654.

Schlatter, P. & Örlü, R. 2010 Assessment of direct numerical simulation data of turbulent boundary layers. *J. Fluid Mech.* **659**, 116–126.

Schlatter, P., Örlü, R., Li, Q., Brethouwer, G., Fransson, J. H. M., Johansson, A. V., Alfredsson, P. H. & Henningson, D. S. 2009 Turbulent boundary layers up to $Re_\theta = 2500$ studied through simulation and experiment. *Phys. Fluids* **21** (051702).